REVISTA INTERDISCIPLINAR DE PESQUISA EM ENGENHARIA

CILAMCE 2016
XXXVII IBERIAN LATIN AMERICAN CONGRESS ON COMPUTATIONAL METHODS IN ENGINEERING
BRASÍLIA - DF - BRAZIL

A THERMOELASTIC ANALYSIS USING THE BOUNDARY ELEMENTS, DIC AND THERMAL IMAGES

Matheus B. A. M. Oberg

Carla T. M. Anflor

matheus.oberg@gmail.com

anflor@unb.br

University of Brasília

Área Especial de Indústria, Projeção A, Gama Leste, Brasília, 72444- 240, DF, Brazil

Abstract. *The main goal of this work relies on developing an experimental procedure to verify a thermoelastic Boundary Elements Method (BEM) analysis using imaging techniques for obtaining the steady-state displacement and temperature fields on isotropic solids. The experimentally obtained temperature field is used as input for the numerical BEM analysis in order to represent the thermal expansion effect. The domain's temperature and consequent resultant thermoelastic displacement fields are carried into the BEM formulation using the Radial Integration Method (RIM). This method consists in a mathematical technique where the radial basis functions are applied to convert domain integrals to the boundary. The use of the RIM avoids the necessity of domain discretization and, therefore, preserves the BEM advantages. For this method to be effective, the experimentally obtained field that describes the temperature difference between the initial and final temperatures on the domain is described by a forth order polynomial. In the end, the resultant numerical displacement field, obtained from the experimental temperature field and the BEM analysis, is compared to the experimental displacement data in order to evaluate the numerical method efficacy. The verified proximity between the obtained numerical displacement curves and its experimental equivalents indicates the good performance of the proposed methodology.*

Keywords: *Boundary elements, Thermoelasticity, Digital image correlation, Thermal images.*

1 INTRODUCTION

The thermoelastic effect has always been a subject of great importance in modern societies. Many important machines operate constantly under the effect of thermal loadings that must be precisely considered in their projects in order to ensure its safety and effectivity. The complexity growth in the projects experienced in last few decades, also compelled the development of Computer Assisted Engineering (CAE) and the search for better numerical tools and more efficient numerical tools.

In this context, the Boundary Element Method (BEM) arose as an alternative for the already well established numerical methods, such as the Finite Element Method (FEM). Its main feature lies in the discretization reduced exclusively to the boundaries of the domains, valued in many engineering situations, such as problems that require constant remeshing and problems involving infinite domains.

Given its importance to engineering, the thermoelastic BEM formulation was probably one of the earliest BEM formulations to be developed. Detailed in Sládek and Sládek (1983) and in Sládek and Sládek (1984), the thermoelastic BEM shares some similarities with the BEM formulation considering the presence of body forces. In this sense, the thermoelastic contribution term also naturally arises in the formulation as a domain integral. At first, the presence of a domain term in a BEM formulation contradicts its main feature, once it supposedly requires domain discretization. However, in face of that problem, several different techniques have been developed to convert these kinds of terms into boundary equivalents and preserve BEM's benefits. In early efforts, Cruse (1975) presented a solution for centrifugal loadings based on the divergence theorem, while, Danson (1981) proposed an alternative solution for centrifugal and gravitational loadings based on the Galerkin vector and the Gauss-Green theorem. The search for a more general method to deal with the domain terms led to development of the Dual Reciprocity Method (DRM) presented in Nardini and Brebbia (1983) and detailed in Partridge et al. (1992). This method relies in the use of Radial Base Functions (RBF) to approximate the effects of the body forces. Aiming the solution of the Helmholtz and Poisson equations, Nowak and Brebbia (1989) introduced the Multiple Reciprocity Method. It had its application extended to the solution of the Navier equation for elasticity in Neves and Brebbia (1991) and to any body force in Ochiai and Kobayashi (1999).

More recently, Gao (2002) proposed a purely mathematical alternative to convert domain integrals of any kind into boundary integral equivalents: the Radial Integration Method (RIM). In Gao (2003) this technique was applied in the thermoelastic BEM formulation in order to obtain a boundary-only integral equation. It also presented a validation procedure based on an analytical solution known for a specific case of a temperature field already described as a function. In most real engineering cases, the temperature field is obtained in the form of punctual temperature values instead of a function and, therefore, require a fitting procedure to convert the obtained set of punctual values into a function that approximates it properly. For these cases, a validation procedure is also needed in order to ensure the applicability of the chosen approximation function.

A verification procedure using thermal images is presented in Dondero et al. (2011) for the potential BEM formulation used to model a steady-state heat transfer problem in a porous domain. This procedure relied in thermal images to capture the temperature field acting over the surface of a test subject. To verify a thermoelastic formulation, in addition to the temperature field, information regarding the resultant displacement field is also needed. In face of this, Silva and Ravichandran (2011) and Bodelot et al. (2009) proposed experimental assemblies in which thermal imaging was employed to obtain the acting temperature fields at

the same time that the resultant displacement fields were evaluated by the means of a Digital Image Correlation (DIC) analysis.

In accordance with Pan et al. (2009), the DIC analysis is an optical metrology technique capable of providing full-field displacement solutions for a surface based on the comparison of digital images taken before and after the application of a deformational load. This method requires the measured surface to be previously marked with a random speckle pattern necessary for the correlation procedure. In face of the direct influence of the chosen speckle pattern on the DIC results, several works, such as Lecompte et al. (2006a), and Lecompte et al. (2006b), presented studies on optimized speckle pattern parameters.

While the DIC analysis requires the surface to have a good contrast between the speckle pattern and the background surface, the thermal images analysis accuracy depends on the uniformity of the measured surfaces. As evinced in Silva and Ravichandran (2011) and also in Bodelot et al. (2009), these contrasting surface preparation requirements pose a significant obstacle for the simultaneous use of both techniques. In both these works, the experimental analysis relied in the use of specially developed coatings capable of creating the speckle pattern necessary to the DIC analysis with minor interference in the thermal images.

Inspired on the aforementioned studies, this work proposes an alternative experimental assembly and procedure for the verification of the BEM formulation for thermoelasticity proposed in Gao (2003) considering temperature inputs, initially, in the form of a set of punctual temperature values. The presented experimental assembly avoids the need for any special coatings, since it uses different faces of a thin plate to acquire the DIC and the thermal images.

2 BOUNDARY ELEMENTS METHOD FOR THERMOELASTICITY

The Boundary Elements Method (BEM) is a numerical analysis method characterized by its boundary-only solution approach. Since its early development in the 1980's, a huge effort has been done in order to broaden its application in engineering problems and provide an alternative to domain methods such as the Finite Elements Method (FEM). The absence of a domain discretization provided by the BEM, which reduces its discretization procedure to the boundaries of the analyzed domain, can promote significant computational efficiency for problems that require constant remeshing and/or involve infinite domains, for example.

In many engineering problems, body forces, such as self-weight and thermoelastic stresses, arise naturally in the numerical formulation as domain terms. Given the boundary-only characteristic of the BEM, at a first sight, the presence of such terms compromise this method's main feature. In face of this, many different techniques have also been developed along with the BEM to treat this problem specifically and convert domain integrals to equivalent expressions described over the boundaries of its domains. In a recent effort, Gao (2002) presented the Radial Integration Method (RIM), a technique that converts domain integrals into boundary equivalents based on an exclusively mathematical procedure. The conversion procedure presented in this work is defined by the equation:

$$\int_{\Omega} f(x_1, x_2) d\Omega = \int_{\Gamma} \frac{1}{r(q)} . \frac{\partial r}{\partial n} . F(q) . d\Gamma \tag{1}$$

where:

$$F(q) = \int f(x_1, x_2) r dr \tag{2}$$

Many of the most common engineering problems involving thermoelastic stresses and deformations can be satisfactorily modelled by the means of steady-state thermoelastic numerical formulation. In the BEM formulation for such natured problems displayed in equation (3) and presented in several books, such as Aliabadi (2002), Katsikadelis (2002) and Banerjee (1981), the thermoelastic contribution term arises as a domain integral.

$$c_{ij}u_j + \int_\Gamma (T_{ij}u_j - U_{ij}t_j)d\Gamma = \int_\Omega U_{ij,j} k\theta d\Omega \tag{3}$$

for:

$$U_{ij} = \frac{1}{8\pi(1-\nu)G}\left[-(3-4)\delta_{ij}\ln(r) + r_{,i}r_{,j}\right] \tag{4}$$

$$T_{ij} = \frac{-1}{4\pi r(1-\nu)}\left\{\frac{\partial r}{\partial n}\left[(1-2\nu)\delta_{ij} + 2r_{,i}r_{,j}\right] - (1-2\nu)(r_{,i}n_j - r_{,j}n_i)\right\} \tag{5}$$

Following Gao (2003) and applying the RIM technique to the domain term in equation (3) results in:

$$\int_\Omega U_{ij,j} k\theta d\Omega = \int_\Gamma \frac{1}{r(q)}\frac{\partial r}{\partial n}\left(\frac{-(1+\nu)k}{2\alpha\pi(1-\nu)} r_{,i}\bar{F}(q)\right) d\Gamma \tag{6}$$

Substituting equation (6) directly into equation (3) results in the boundary exclusive integral formulation for the steady-state thermoelastic problem:

$$c_{ij}u_j + \int_\Gamma (T_{ij}u_j - U_{ij}t_j)d\Gamma = \int_\Gamma \frac{1}{r(q)}\frac{\partial r}{\partial n}\left(\frac{-(1+\nu)k}{2\alpha\pi(1-\nu)} r_{,i}\bar{F}(q)\right) d\Gamma \tag{7}$$

3 DIGITAL IMAGE CORRELATION AND THERMAL IMAGES

The DIC method, detailed in Pan et al. (2009), is a non-destructive experimental method capable of providing full field solutions for superficial deformation. To do so, this method relies in the comparison between digital images of the target surface taken before any deformational load is applied and after. The target surface must be marked beforehand with a randomly distributed speckle pattern, which is used as a reference for a mapping procedure performed on the non-deformed surface image. This mapping procedure, illustrated in figure

(1), divides the marked surface into a subset of smaller regions and creates a physical point associated to each new sub-region. In a monochromatic scale, each pixel can be associated to a discrete intensity value, f(x,y), that is translated into a shade of gray. In this sense, the speckle pattern contained in each sub-regions creates an individual identity for it based on its associated intensity values.

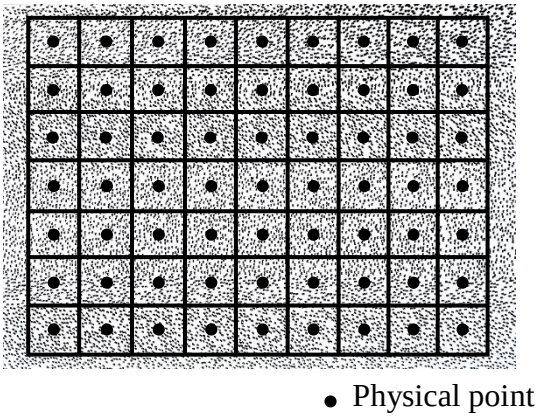

Figure 1. DIC mapping procedure.

When the marked surface is mechanically loaded, the marked pattern is deformed and distorted with the surface itself. Consequently, the mapped subsets are also displaced and have its boundaries deformed as illustrates figure (2).

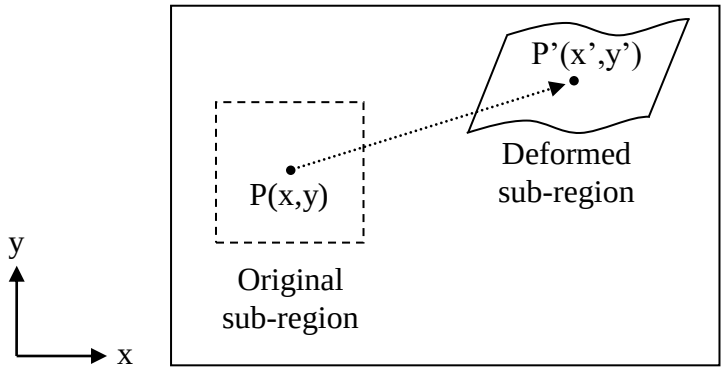

Figure 2. Sub-region deformation.

Based on the marked pattern present in each sub-region, a correlation analysis is performed to identify the deformed equivalents of each sub-region in the deformed images. By doing so, it is possible to assess de deformation and distortion suffered by each sub-region and, hence, by each physical point. For the correlation step, two types of approaches are commonly used: the cross-correlation (CC) and the sum-squared differences (SSD) equations. Variations of both types of equations are displayed in equations (8) and (9).

$$CC_{normalized} = \frac{\sum\left[f(x,y).g(x,y)\right]}{\left[\sum f(x,y)^2\right]^{1/2}.\left[\sum g(x,y)^2\right]^{1/2}} \tag{8}$$

$$SSD_{normalized} = \sum\left\{\frac{f(x,y)}{\left[\sum f(x,y)^2\right]^{1/2}} - \frac{g(x,y)}{\left[\sum g(x,y)^2\right]^{1/2}}\right\}^2 \tag{9}$$

In both these equations, f(x,y) and g(x,y) are the intensity functions for the reference non-deformed surface and deformed surface images respectively. In the end, based on the correlation results, the deformational solution is calculated for the physical points and interpolated for other parts of the analyzed domain.

4 EXPERIMENTAL ANALYSIS

An experimental assembly was elaborated in order to assess the results provided by the proposed BEM formulation using the DIC analysis and thermal images simultaneously. The combined use of these optical methods had already been performed in works such as Silva and Ravichadran (2011) and Bodelot et al. (2009) for different purposes. Both these works evince the challenges of using DIC simultaneously with thermal images to evaluate the same surface due to the contrasting surface preparation requirements involved. While the DIC requires the surface to have a random speckle pattern marked over it, the thermal images heavily benefit in the uniformity of the surface. To overcome this issue, in this work, an experimental assembly was elaborated, in which an aluminum thin plate was placed vertically over a heater. In this sense, instead of aiming both optical methods to the same surface, it was possible to take the thermal images at one side of the plate while the DIC images were taken at the opposite side. Given the small thickness of the plate, both information could be superimposed later to compose the complete thermoelastic problem. The proposed experimental assembly is schematized in figure (3).

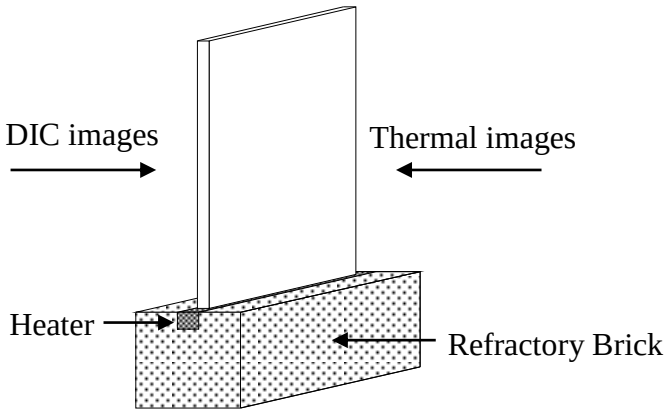

Figure 3. Schematic drawing of the experimental assembly.

4.1 Materials used in the proposed assembly

The proposed experimental assembly used the following materials:

- 1 ASTM 6351 aluminum alloy plate measuring 140 x 102 x 9.6 mm;
- 1 high wattage cartridge heater with 3/8" diameter and 140 mm of useful length;
- 1 refractory brick used as support for the heater;
- Dantec Dynamics' Q-400 DIC system;
- Fluke's Ti 125 30 Hz thermal imager.

4.2 Test subject preparation

The chosen test subject for the verification procedure was an ASTM 6351 aluminum alloy plate measuring 140 x 102 x 9.6 mm. In face of the different surface requirements imposed by the DIC, the thermal imaging procedure, and the proposed experimental assembly, each face of the plate was prepared differently. Following the surface preparation for thermal imaging presented in Dondero et al. (2011), the surface chosen to provide the thermal image was painted matte black in order to increase the uniformity of its emissivity. To satisfy the DIC requirements, the opposite side of the plate was prepared in two layers. Initially, the whole surface was painted matte white in order to eliminate the aluminum's characteristic reflectivity and to increase the contrast with the speckle pattern marked as a second layer. To ensure good speckle pattern parameters based on the results presented in Lecompte et al. (2006a), Lecompte et al. (2006b), Pan et al. (2008), and Barranger et al. (2010) and Crammond et al. (2011), a numerically generated random speckle pattern was marked with the aid of a CNC marking device specially developed for this task. The generated pattern obeyed a 40% area ratio occupied by the speckles and granted relatively uniform speckle distribution along the surface. The marked surface obtained at the end of the process is presented in figure (4).

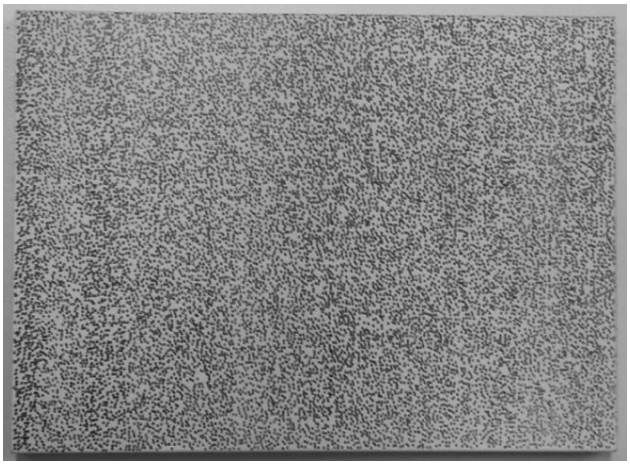

Figure 4. Speckle pattern marked over the surface for the DIC analysis.

4.3 Experimental procedure

The proposed experimental procedure consisted of three main stages: the reference, the heating, and the steady-state acquisition steps. The reference step is the first one and is performed before the plate is heated. At this stage, an initial DIC image, without any displacements, was taken to serve as a reference for the DIC analysis. A thermal image was also taken in order to ensure that the initial temperature field acting at the plate was constant and equal to the room temperature at that time. After that, the heating acquisition step, in which the base of the plate was uniformly heated, took place. The whole heating process was continuously monitored by means of thermal images in order to determinate whether or not the steady-state condition is achieved. When the steady-state condition was reached, the last stage of the procedure, the steady-state images acquisition, was performed. At this point, a new set of thermal and DIC images was taken.

4.4 Experimental results

Comparing the thermal images taken at the reference and the steady-state acquisition steps it was possible to obtain the temperature field resultant of the heating procedure. A graphical display of this temperature field is presented in figure (5). In this figure, the blue circles represent the local temperature gains based on the local differences between the reference and steady-state thermal images. The other parts of the temperature field displayed were interpolated from these local values using a fourth-order polynomial fit.

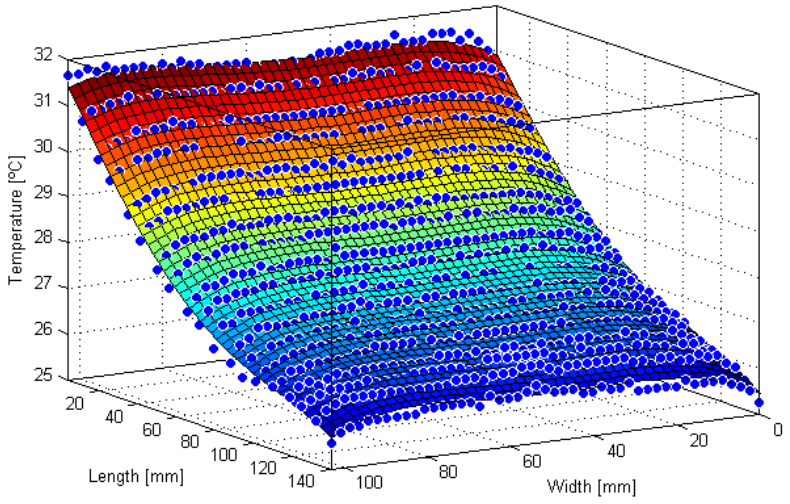

Figure 5. Temperature field caused by the heating procedure.

The performed DIC analysis provided displacement solution for over 1600 physical points, proving the good performance of the used speckle pattern. In face of the small dimensions of the measured surface, this amount of physical points allowed a relatively accurate analysis of the resultant displacement fields. Figures (6) and (7) graphically present the displacement fields obtained via DIC analysis in the x_1 and the x_2 directions, respectively, due to the heating.

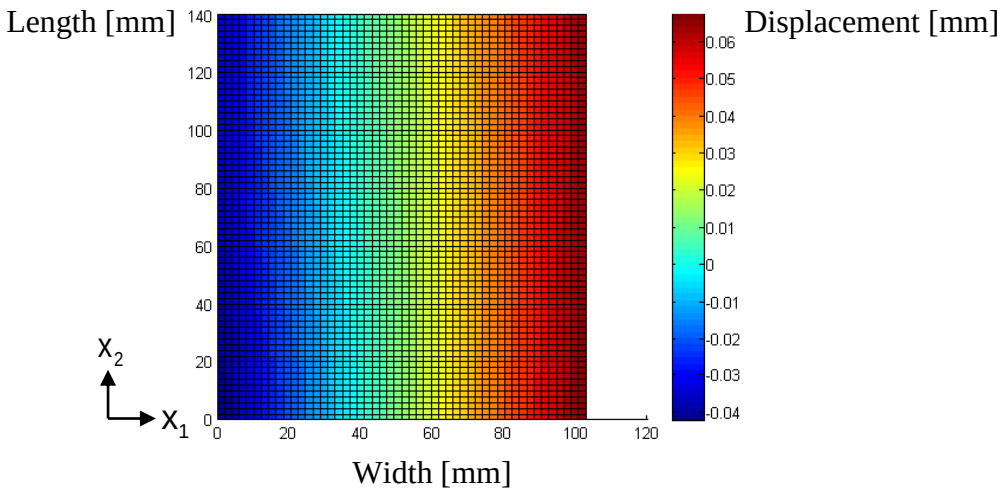

Figure 6. Graphical representation of the displacement field over the plate in regards to the x_1 direction.

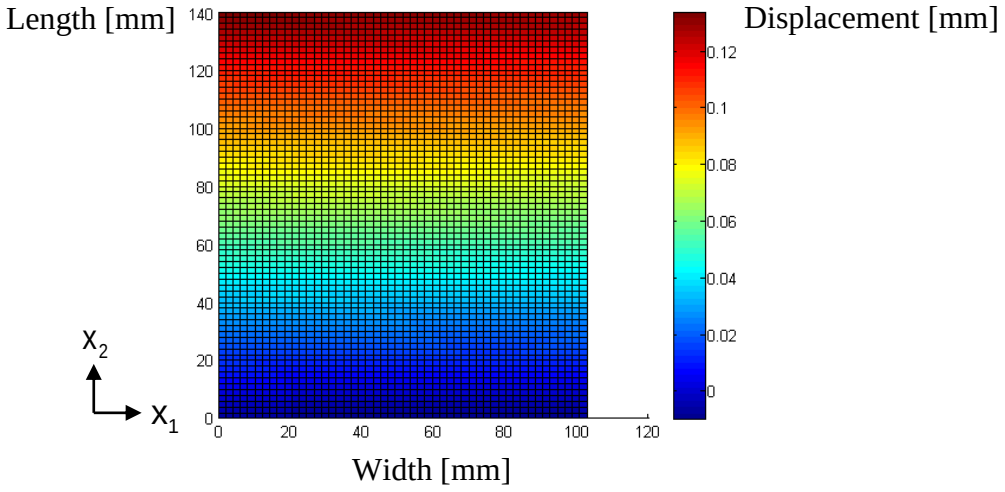

Figure 7. Graphical representation of the displacement field over the plate in regards to the x_2 direction.

5 VERIFICATION PROCEDURE

In face of the experimental results obtained, the first step in the verification procedure consists in numerically replicating the experimental condition using the thermoelastic BEM formulation obtained with the RIM. In this sense, the plate used in the experiment is modelled as a bidimensional rectangular domain discretized into 42 equally spaced quadratic boundary elements. As boundary conditions, the displacement along the bottom edge of the model had the displacement in x_2 direction constrained while a single physical node of an element at this edge had its displacement in the x_1 also constrained in order to satisfy the static balance equation in this direction. The location of this node is coincident with the position in the experimental results where the displacement in the x_1 direction approximates 0. After these constraints were set, the next step was to input the thermal load observed in the experiment into the numerical model. The thermoelastic formulation obtained from the RIM requires the

temperature field originated from the heating to be input as a single function. However, the thermal image analysis could only provide punctual temperature values, therefore the punctual temperature values obtained experimentally were approximated by a fourth-order polynomial function using a fit procedure.

To better assess the accuracy of the proposed methodology and enable a clear graphical evaluation, it was adopted an approach in which the numerically obtained results were compared to numerical results over three horizontal lines placed as depicted in figure (8). For each line, two types of errors were calculated based on the difference between the numerical and experimental results: the maximum absolute error and the root mean square (RMS) error. The first one has the goal of evaluating the error variation along the lines, while the RMS was chosen to verify the error difference between each verification line. The error values obtained for each displacement components at the lines (a), (b) and (c), as placed in figure (8), are displayed in tables (1) and (2). Graphical comparisons between the numerical and experimental results for the x_1 and x_2, respectively, are shown in the figures (9) and (10).

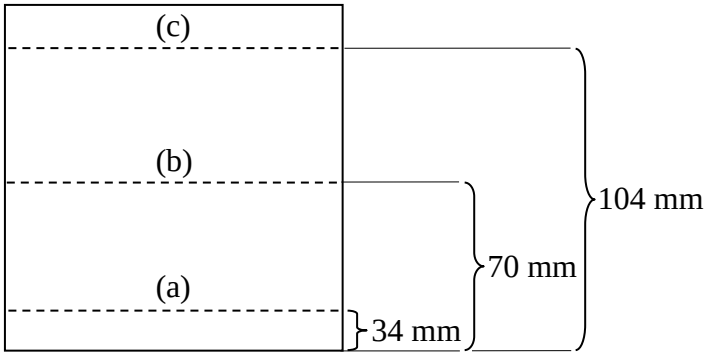

Figure 8. Positioning of the verification lines.

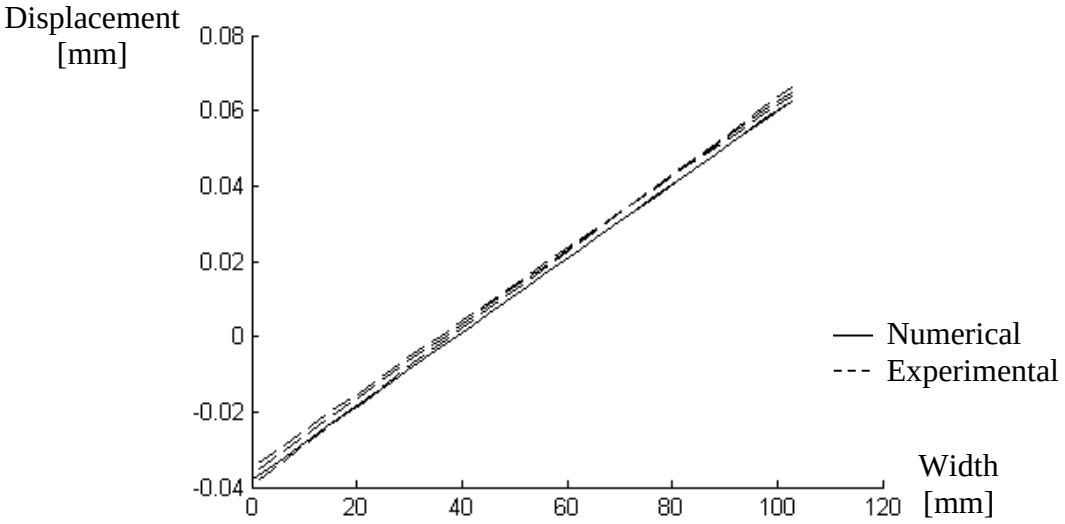

Figure 9. Numerical and experimental displacements in the x_1 direction for lines (a), (b) and (c).

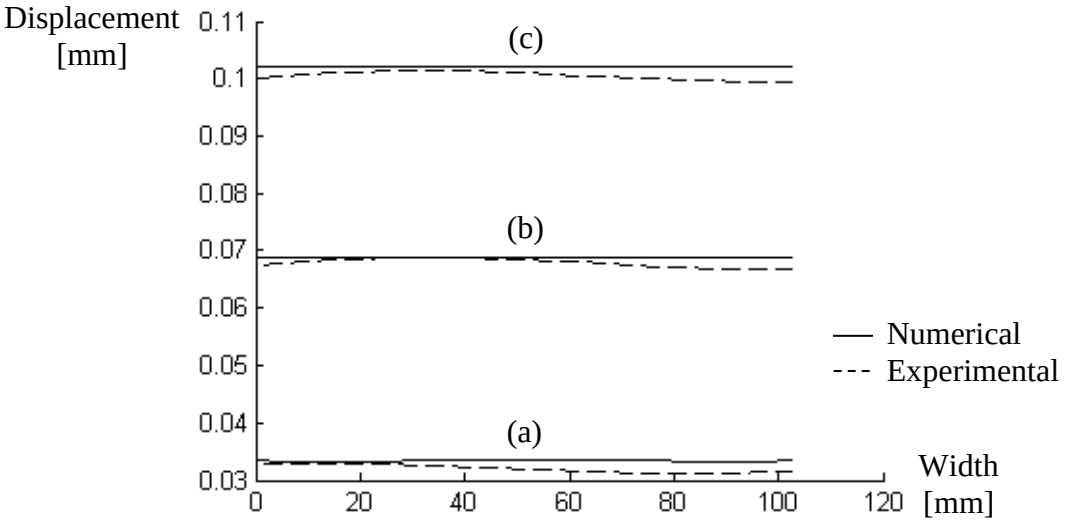

Figure 10. Numerical and experimental displacements in the x_2 direction for lines (a), (b) and (c).

Table 1. Maximum and RMS errors for the displacement along the x_1 direction for lines (a), (b) and (c).

Line	Maximum error [mm]	RMS error [mm]
(a)	0.0036	0.0020
(b)	0.0024	0.0022
(c)	0.0033	0.0028

Table 2. Maximum and RMS errors for the displacement along the x_2 direction for lines (a), (b) and (c).

Line	Maximum error [mm]	RMS error [mm]
(a)	0.0022	0.0015
(b)	0.0019	0.0011
(c)	0.0026	0.0017

5.1 Result analysis

The graphical analyses presented in figures (9) and (10) show already a good proximity between the numerical and experimental results. The proximity of the curves obtained for the displacements along the x_1 direction, displayed in figure (9), rendered it impossible to clearly distinguish the results for lines (a), (b) and (c). Such behavior was already expected due to the linear behavior also observed for the x_1 direction in figure (8). In a similar way, the almost flat aspect of the curves obtained in figure (10) were also expected due to the linear behavior observed along the x_2 direction in figure (9).

Focusing on the error results displayed in tables (1) and (2) it is possible to notice that for both cases the line placed at the center of the plate provided the most accurate results. In spite of the matte black paint coating applied to the surface used for the thermal image acquisition, the surface is still susceptible to reflection issues caused by environmental diffuse and

background lighting. These effects are more influent at regions closer to the edges of the plate, explaining the higher RMS errors on lines (a) and (c) and also the slight absolute error increase observed in figure (10) at regions closer to lateral edges. However, the error variation observed is still small in comparison to the order of the magnitude of the overall error obtained, which is compatible with the measurement resolution limitations of the equipment used for the data acquisition.

6 CONCLUSION

This work developed an experimental methodology created to verify the accuracy of the thermoelastic BEM formulation based on the RIM. It consisted in a steady-state thermoelastic experimental analysis based on simultaneous DIC and thermal images acquisition. In order to allow a comparison between the numerical and the experimental results, the experimentally observed condition was then numerically replicated using the aforementioned BEM formulation. In the end, the small magnitude order of the obtained error values and, hence, good agreement between the numerical and experimental displacement fields pointed out for the good performance of the numerical methodology. The compatibility of the obtained error values with the measurement resolution limitation of the optical equipment used also points out for the effectiveness of the proposed verification procedure.

ACKNOWLEDGEMENTS

Funding: This work was supported by the Conselho Nacional de Desenvolvimento Científico e Tecnológico (CNPq) of Brazil; and the Coordenação de Aperfeiçoamento de Pessoal de Nível Superior (Capes) of Brazil.

REFERENCES

Aliabadi, M.H., 2002. The Boundary Element Method, Volume 2, Applications in Solids and Structures. Wiley.

Banerjee, P., & Butterfield, R., 1981. Boundary elements method in engineering science. Mcgraw-hill.

Barranger, Y., Doumalin, P., Dupré, J.C., Germaneau, A., 2010. Digital image correlation accuracy: Influence of kind of speckle and recording setup. *EPJ web of conferences Volume 6 - ICEM 14 – 14th International Conference on Experimental Mechanics.*

Bodelot, L., Sabatier, L., Charkaluk, E., & Dufrénoy, P., 2009. Experimental setup for fully coupled kinematic and thermal measurements at the microstructure scale of an AISI 316L steel. *Materials Science and Engineering A*, vol. 501, pp. 52-60.

Crammond, G., Boyd, S.W., & Dulieu-Barton, J.M., 2013. Speckle pattern assessment for digital image correlation. *Optics and Lasers in Engineering*, vol. 51 n. 12, pp. 1368-1378.

Cruse, T. A., 1975. Boundary integral equation method for three-dimensional elastic fracture mechanics. *AFOSR-TR-75-0813, ADA 011660*. Pratt and Whitney Aircraft-Connecticut.

Danson, D.J., 1981. A boundary element formulation for problems in linear isotropic elasticity with body forces. In Brebbia, C.A., ed, *Boundary Element Methods*, Berlin, pp. 105–122. Springer-Berlin.

Dondero, A., Cisilino, A.P., Carella, J.M., & Tomba, J.P., 2011. Effective thermal conductivity of functionally graded random micro-heterogeneous materials using representative volume element and BEM. *Intenational Journal of Heat and Mass Transfer*, vol. 54 n. 17-18 pp. 3874-3881.

Gao, X.W., 2002. The radial integration method for evaluation of domain integrals with boundary-only discretization. *Engineering Analysis with Boundary Elements*, vol. 26, pp. 905-916.

Gao, X.W., 2003. Boundary element analysis in thermoelasticity with and without internal cells. *International Journal for Numerical Methods in Engineering*, vol. 57, n. 7, pp. 975-990.

Katsikadelis, J.T., 2002. Boundary elements: Theory and Applications. Elsevier, Oxford.

Lecompte, D., Sol, H., & Vantomme, J., 2006. Analysis of speckle patterns for deformation measurements by digital image correlation. *Proceedings of SPIE vol. 6341, Speckle06, From Grains to Flowers*.

Lecompte, D., Smits, A., Bossuyt, S., Sol, H., Vantomme, J., Van Hemelrijck, D., & Habraken, M.A., 2006. Quality assessment of speckle patterns for digital image correlation. *Optics and Lasers in Engineering*, vol. 44, n. 11, pp. 1132-1145.

Nardini, D., & Brebbia, C.A., 1983. A new approach for free vibration analysis using boundary elements. *Applied Mathematical Modelling*, vol. 7, n. 3, pp.157-162.

Neves, C.A., & Brebbia, C.A., 1991. The multiple reciprocity boundary element method in elasticity: a new approach for transforming domain integral to the boundary. *International Journal for Numerical Methods in Engineering*, vol. 31, n. 4, pp. 709–27.

Nowak, J.A., & Brebbia, C.A., 1989. The multiple-reciprocity method. A new approach for transforming B.E.M. domain integrals to the boundary. *Engineering Analysis with Boundary Elements*, vol. 6, n. 3, pp. 164–167.

Ochiai, Y., & Kobayashi, T., 1999. Initial stress formulation for elastoplastic analysis by improved multiple-reciprocity boundary element method. *Engineering Analysis with Boundary Elements*, vol. 23, pp. 167–73.

Pan, B., Qian, K., Xie, H., & Asundi, A., 2008. On errors of digital image correlation due to speckle patterns. *Proceedings of ICEM 2008: International Conference on Experimental Mechanics.*

Pan, B., Qian, K., Xie, H., & Asundi, A., 2009. Two-dimensional digital image correlation for in-plane displacement and strain measurement: A review. *Measurement Science and Technology*, vol. 20, n. 6, pp.1-17.

Partridge, P.W., Brebbia, C.A., & Wrobel, L.C., 1992. The Dual Reciprocity Boundary Element Method. Computational Mechanics Publications.

Silva, M.L., & Ravichandran, G., 2011. Combined thermoelastic stress analysis and digital image correlation with a single infrared camera. *Journal of Strain Analysis for Engineering Design*, vol. 46, n. 8, pp. 783-793.

Sládek, V., & Sládek, J., 1983. Boundary integral equation in thermoelasticity, Part I: General analysis. *Applied Mathematical Modelling*, vol. 7, n. 4, pp. 241-253.

Sládek, V., & Sládek, J., 1984. Boundary integral equation in thermoelasticity, Part III: Uncoupled thermoelasticity, *Applied Mathematical Modelling*, vol. 8, n. 6, pp. 413-418.